Improving sea ice type discrimination by the simultaneous use of SSM/I and scatterometer data

Stefan Voss, Georg Heygster & Robert Ezraty

The multi-year sea ice (MY) concentration as determined with the NASA Team algorithm (NTA) shows an increase during winter. This unrealistic feature can be reduced using combined active and passive remote sensing data, leading to a more realistic estimation of MY area. Our joint analysis of SSM/I, QuikSCATterometer (QSCAT) and meteorological data reveals events (i.e. intervals in space and time) where increased surface roughness and volume scattering, after a melt–refreezing episode, alters the passive microwave signature of the undisturbed sea ice surface. In these events, the calculation of MY and FY areas employing the NTA leads to false estimations of their amounts. It is shown that when such events occur, QSCAT backscatter values increase by more than 3 dB. This backscatter variation can be easily detected and the FY and MY area determination of the NTA can be corrected accordingly within defined event–regions. Using this method, called Simultaneous NTA, we found that in May 2000 12% of the area detected by the NTA as MY has to be corrected to FY. As a consequence, a detailed reanalysis of the 20-year passive microwave data set is suggested to more precisely compute the MY area.

S. Voss & G. Heygster, Institute of Environmental Physics, University of Bremen, Box 330440, D-28334 Bremen, Germany, heygster@uni-bremen.de; R. Ezraty, Institut Français de Recherche pour l'Exploitation de la Mer, Centre de Brest, BP 70-29280 Plouzané, France.

In the context of climate scenarios, perennial sea ice volume is a major prognostic parameter used by modellers to detect long-term warming trends in the Arctic. When used for control purposes, this parameter is in practice reduced to multi-year sea ice (MY) extent obtained from microwave satellite measurements because of the scarcity of sea ice thickness measurements. The multifrequency brightness temperature (TB) data of the Scanning Multichannel Microwave Radiometer (SMMR) and the later Special Sensor Microwave/Imager (SSM/I) are used to calculate the ice concentration (the percentage of ice-covered ocean). Analysis of this data over the period 1978–1997 reveals a reduction of about 3% per decade in total ice extent (Parkinson et al. 1999; Serreze et al. 2000). But it has remained unclear whether the amount of MY (ice having survived at least one summer season) has changed. On average, MY is about three times thicker than first-year ice (FY)—which is typically 1-2 m thick—so that changes in ice type distribution are important climate change indicators. Evidence of a long-term trend of the sea ice cover has been presented by Johannessen et al. (1999) by analysing time series of MY areas from 1979 to 1998, based on SMMR and SSM/I data (see their Fig. 1). On the one hand, this figure shows a trend of 14% reduction of the MY area during this 19-year period. On the other hand, during the winter period, a large increase in MY is shown, which is unrealistic since all increase is FY. Kwok et al. (1996) have shown that the variability in MY during winter appears to be caused by spatial and temporal variations in the signatures assumed constant in the algorithm, but they

did not identify the responsible geophysical processes.

MY, FY and open water have different radiative properties. The NASA Team algorithm (NTA) developed for the SMMR instrument (Gloersen et al. 1992) and later revised to be used for the SSM/I data (Cavalieri et al. 1991) is able to separate each of these surface types and estimate the FY and MY concentrations (C_{FY} and C_{MY}) in the cold season. Although the total ice concentrations (C_T) estimated as $C_{FY} + C_{MY}$ seems realistic, sudden, unrealistic variations of opposite sign in C_{FY} and C_{MY} time series have limited the confidence in these estimates.

The purpose of this paper is to show how the use of independent external information, namely the variations of backscatter measured by a scatterometer, can be used to identify the intervals in time and space (hereafter "events") when passive radiometer measurements will lead to a false MY concentration value.

The data sets and the basic parameters used are presented in the following section. We then discuss an illustrative example of an event, after which we present the method used to detect systematically these events and then correct the ice concentration.

The data sets

The radiometric data and the NTA

Since 1987, the SSM/I radiometer onboard the USA's Defense Meteorological Satellite Program satellite series measures brightness temperatures at different frequencies and polarizations (V polarization and H polarization) at a constant incidence angle of 53° (Hollinger et al. 1990). The NTA makes use of the channels measuring at 19 GHz vertical and horizontal polarization (19 V, 19 H) and at 37 GHz vertical polarization (37 V). The data are processed and mapped onto a 25×25 km^2 polar stereographic grid prepared by the National Snow and Ice Data Center (NSIDC). The algorithm exploits the large brightness temperature difference of open water and ice between the 19 V and 19 H channels. Furthermore, the T_B difference between 37 V and 19 V is greater over MY than over FY. These properties are expressed in the form of two independent variables: the polarization ratio (PR) and the gradient ratio (GR) defined as:

$$PR = [T_B(19\,V) - T_B(19H)] / [T_B(19\,V) + T_B(19\,H)]$$

$$GR = [T_B(37\,V) - T_B(19\,V)] / [T_B(37\,V) + T_B(19V)]$$

which are the input quantities to the algorithm. Using ratios of T_B reduces the errors due to surface temperature variations. PR is mainly sensitive to C_T while GR varies with the fractions of FY and MY (see Fig. 2.3.5 in Gloersen et al. 1992). Reference T_B (tie points) define, in the PR-GR diagram, the location of 100 % C_{FY}, 100 % C_{MY} and open water. Once the percentage of each ice type is computed, C_T is estimated as:

$$C_T = C_{FY} + C_{MY}.$$

The scatterometer data and the meteorological data

Scatterometers have been originally constructed for wind vector retrieval over the ocean. Yet it has been shown that they provide useful information on sea ice type and extent (Gohin & Cavanié 1994; Ezraty & Cavanié 1999; Bingham & Drinkwater 2000). A scatterometer emits an electromagnetic pulse and measures the backscattered signal. The normalized radar backscatter σ^0, defined as the ratio of scattered power relative to isotropic scattering targets, is characteristic for the scattering target. In this study, data from the SeaWinds sensor of the QuickSCATterometer mission (QSCAT) are employed. QSCAT operates at 13.4 GHz (K_u-band) and has two beams at constant incidence angles of 46° and 54° with H and V polarization, respectively.

A detailed description of the sensor, the data processing and the final daily backscatter maps can be found in Ezraty & Piollé (2001). These maps use the same polar stereographic projection and the same grid size as used by NSIDC for the SSM/I data. This facilitates comparative and simultaneous studies involving both sensors. In this study, the backscatter maps of the inner beam (H polarization) are used because the dynamic range is higher at the lower incidence angle, and the backscatter signal does not depend significantly on the polarization of the incident radation (Ezraty & Cavanié 1999).

Information about the weather conditions in the regions of interest is obtained from coastal weather stations. Maximum and minimum temperatures and the amount of precipitation are extracted from the website of WetterOnline GmbH (2001).

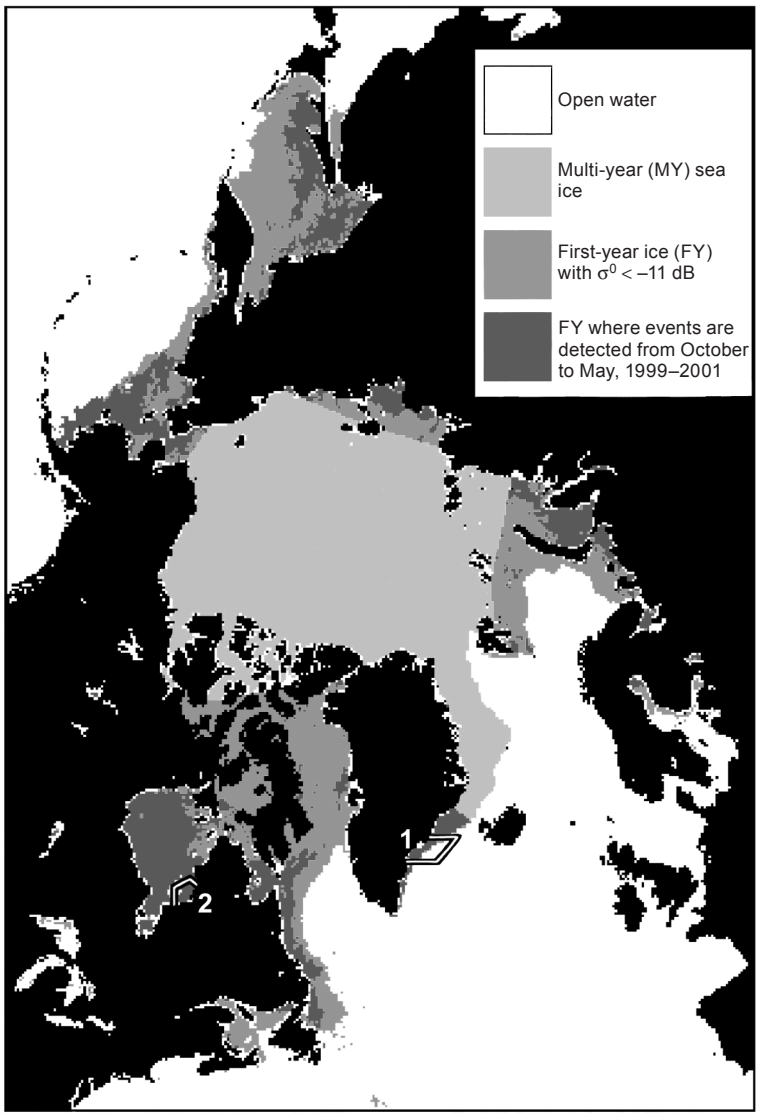

Fig. 1. Map of area showing areas of open water, multi-year sea ice and first-year ice. Investigated areas near Tasiilaq, Greenland (1), and near Kuujjuarapik (2), Hudson Bay, are marked.

Joint analysis of SSM/I, QSCAT and meteorological data for a selected event

This section shows the simultaneous use of data collected by the active and passive microwave instruments together with meteorological information.

The two example areas presented here lie off the east coast of Greenland at the latitude of Iceland (area ca. 300×250 km^2) and in Hudson Bay (ca. 250×250 km^2) (Fig. 1). The meteorological conditions measured at the meteorological station of Tasiilaq (65.6° N, 37.6° W) and Kuujjuarapik (55.2° N, 77.5° W) are assumed to be representative of the whole of the two areas.

High backscatter events

During the Arctic winter, typical σ^0 values for FY are between –18 dB and –11 dB, those of MY are above –11dB (Voss 2002). The threshold of –11 dB is similar to the seasonally slightly varying values found by Kwok et al. (1999). Nevertheless, discriminating FY and MY on the basis of a fixed σ^0 threshold is frequently found incorrect in small areas (80 to 500×10^3 km^2) showing

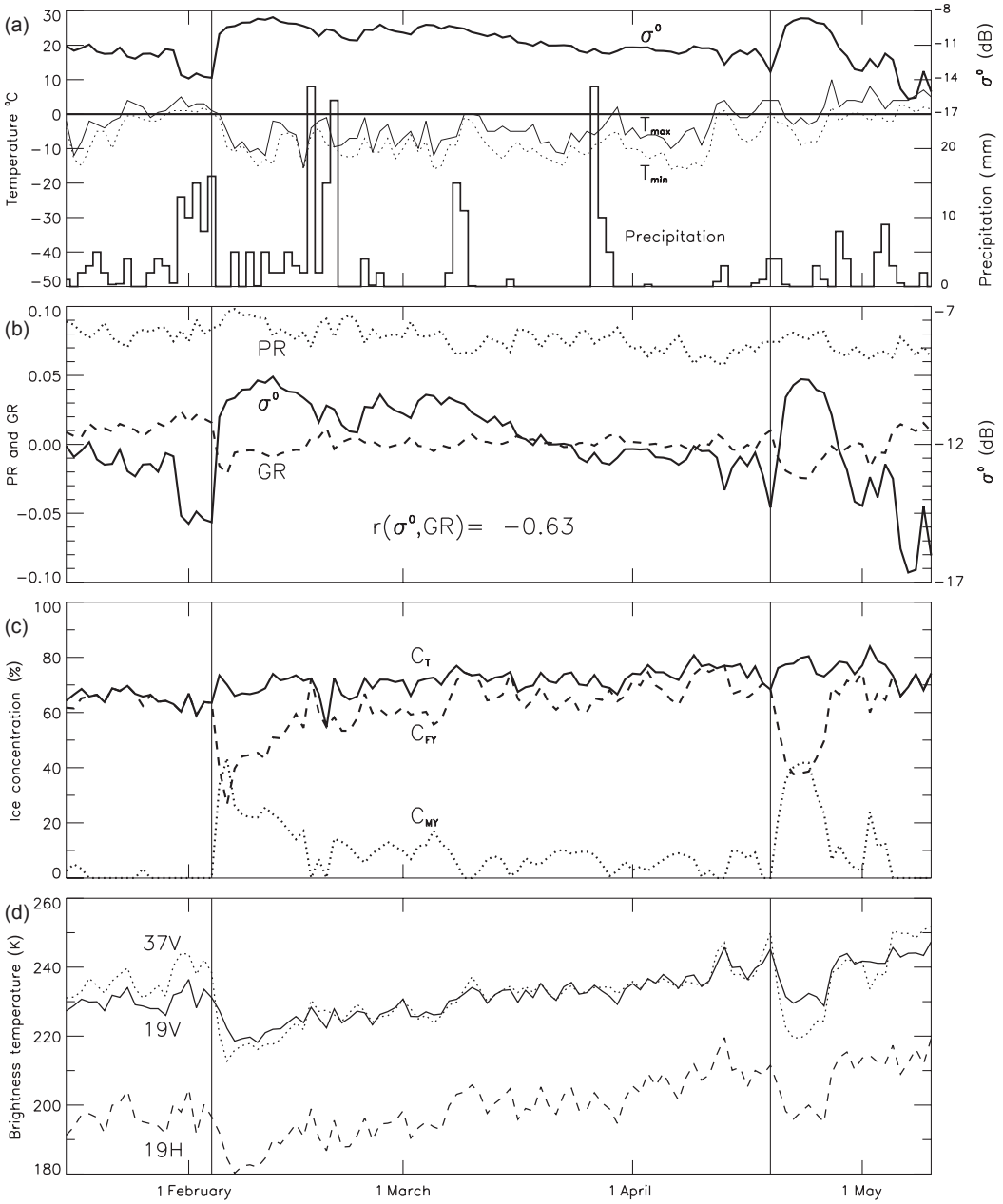

Fig. 2. (a) Time series of daily QSCAT- σ^0 data averaged over the test area off Tasiilaq, Greenland, during 2001 (thick solid line), the daily maximum temperature (T_{max}: thin solid line), minimum temperature (T_{min}: dotted line), and the amount of precipitation (histogram). (b) Time series of QSCAT-σ^0, PR and GR; r is the correlation coefficient between σ^0 and GR. (c) Time series of C_T, C_{MY} and C_{FY} from the NTA. (d) Time series of T_B(19 V), T_B(19 H) and T_B(37 V).

a high σ^0 within ice known to be FY. The time series of the mean σ^0 over the event area marked as number 1 in Fig. 1 is shown in Fig. 2a. Twice during the investigated period, σ^0 increases by about 4 dB within 2-4 days. The beginnings of the σ^0 increases—the "events" (3 February 2001 is event 1 and 20 April 2001 is event 2)—are marked with a vertical bar. The maximum is

reached after 2 and 3 days for event 1 and event 2, respectively. The maximum values of about –9 dB are well within the range of the σ^0 of MY. After event 1, σ^0 decreases slowly over a period of six weeks to the values before the event (<–12 dB), whereas the decrease after event 2 takes only about one week.

To elucidate the mechanism of the events, the time series of daily minimum and maximum air temperatures, and the amount of precipitation as measured at the nearby weather station of Tasiilaq are also displayed in Fig. 2a. Several days before the beginning of both events the daily minimum temperature is above (event 1) or around (event 2) 0 °C with amounts of precipitation between 16 mm (event 1) and 4 mm (event 2). The precipitation is caused by low pressure systems connected to warm air advection. The impact of the weather condition on the microwave properties of the surface is discussed in detail in the next section. Following the warm air advection, cooler and drier weather is observed for event 1, less so for event 2, and σ^0 increases by about 5 dB to values above –9 dB. As will be described later, freezing of liquid water in the snow layer on top of the sea ice leads to strong volume scattering. The volume scattering is further amplified by the snow metamorphosis due to changing temperatures.

Following the first event at the beginning of February, σ^0 decreases slowly and after about four weeks arrives at its previous values. The slow and steady decrease in σ^0 can be explained by the East Greenland Current, which advects sea ice southward along the Greenland coast. With a typical drift of 10 cm/s (Martin & Augstein 2000), the ice in the event region will be exchanged completely by ice coming from the north over a period of about four weeks. This ice was most likely not subjected to a melting–refreezing process because of the high meridional temperature gradient associated with the polar front typically located in this region. The effect of precipitation strongly depends on the surface temperature, as shown in Fig. 2a: while both events are preceded or accompanied by a large amount of wet precipitation (precipitation on days with temperatures above freezing), there is no large increase in σ^0 from dry precipitations (i.e. during periods with temperatures below zero). The fast drop in σ^0 one week after event 2 is due to a new inflow of warm air and rain. Later on, at the end of April and the beginning of May, σ^0 fluctuates increasingly because of the temperature tending to fluctuate around 0 °C causes melt–refreezing cycles, and we observe wet precipitation.

The time series of PR and GR as well as that of σ^0 are presented in Fig. 2b. A slight increase of PR and a strong decrease of GR are observed for both events. Over the depicted time series, GR and σ^0 are anticorrelated with a correlation of –0.63. While no significant variation in the total ice concentration C_T (Fig. 2c) is observed (PR does not change significantly), the changes of GR cause opposite variations in C_{MY} and C_{FY}. C_{MY} increases from 0 % to 40 % and C_{FY} decreases from 65 % to 25 %. The algorithm to determine the ratio between MY and FY is clearly unreliable in this case. A close look at the time series of T_B (Fig. 2d) explains this artefact. Before 3 February the $T_B(37\,V)$ is higher than the $T_B(19\,V)$ ($GR > 0$), but after 3 February the opposite is true. In other words, since the physical surface temperatures are nearly identical, the ratio of the surface emissivities $\varepsilon_{37V}/\varepsilon_{19V}$ has changed from >1 before the event to <1 after the event. Moreover, the simultaneous decrease of T_B by approximately 10 K to 20 K in all three channels tends to increase the absolute values of PR and GR. It follows that the relative fraction of C_{FY} and C_{MY} are significantly modified. It takes about one month for C_{FY} and C_{MY} to reach their previous values, and a similar period for σ^0. As noted earlier, this recovery is mainly due to ice advection, which is a dominant geophysical characteristic of the investigated area. In a previous study of active and passive microwave signatures within the ice pack, Ezraty (1999) used a Lagrangian approach (in order to discard advection effects) and showed that typical recovery duration for C_{MY} is about two months.

To detect melt–refreezing events we prefer to use σ^0 instead of GR for several reasons. (1) σ^0 is measured independently of the passive data which are already used to estimate the MY concentration. (2) σ^0 is a physical quantity that can be measured directly. In contrast, GR is a composed quantity (ratio of difference to sum) with not so obvious statistical properties. Especially taking the difference in the nominator increases the noise. (3) As a consequence, the signal to noise ratio of the events is higher for σ^0 than for GR. This is addressed in the following example: the values of σ^0 and GR are investigated at event 1 and during a 59-day period after event 1 between 12 February and 11 April. During this period both quantities are not influenced by any other event (see Fig. 2). The difference signal between σ^0 on

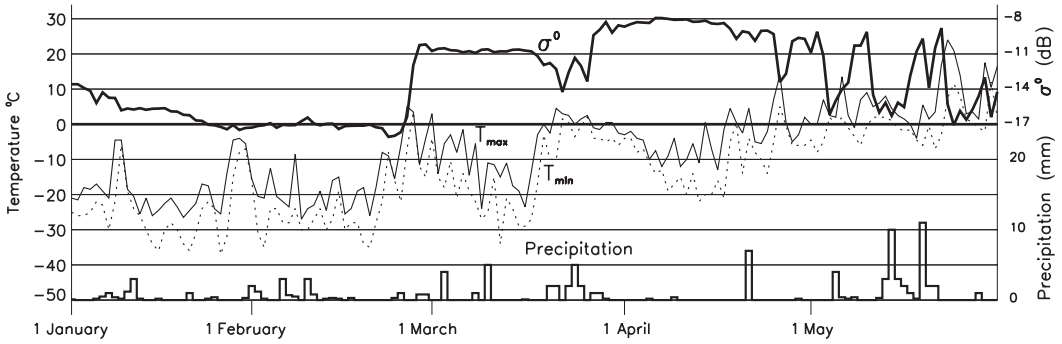

Fig. 3. Time series of daily QSCAT- σ^0 data averaged over the test area off Kuujjuarapik, Hudson Bay) during 2000 (thick solid line), the daily maximum temperature (T_{max}: thin solid line), minimum temperature (T_{min}: dotted line), and the amount of precipitation (histogram).

day *i* and day *i-4* is calculated, similarly for GR. The standard deviations of both difference signals (0.51 dB for σ^0 and 0.0052 for GR) can be related to the leap of σ^0 and GR during event 1 on 3 February (4.4 dB for σ^0 and 0.036 for GR). For σ^0, the leap during the event is 9 times higher than the standard deviation of the differences, but the corresponding ratio of GRs is only 6. 4) The brightness temperatures, especially at 37 GHz, can also be influenced by both cloud liquid water and cloud ice, as has been demonstrated by Liu & Curry (2003). We conclude that σ^0 is more suitable to detect events than GR. It should be noted, however, that other authors have used temporal information of passive microwave measurements to detect thaw–freeze events, e.g. the onset of melt over sea ice (Smith 1998).

Figure 3 shows the time series of the daily backscatter coefficient σ^0 of region 2, and the minimum and maximum temperatures and precipitation at Kuujjuarapik in the year 2000. The correlation of increase of backscatter with wet precipitation is confirmed and permits the identification of the starting dates of three events: 23 February, and 20 and 24 March. After the strong increases associated with the first and last event, σ^0 remains high with small variations. We explain this different behaviour with the fact that the ice in the Hudson Bay is fast and is not drifting slowly out of the event region as in region 1, confirming our finding that the slow decreases of σ^0 after the large increases in Fig. 2a are caused by ice drift and not by ice evolution. The slight decrease of σ^0 around 18 April during the third event is attributed to melting conditions and precipitation around this date, but σ^0 remains above –11 dB. From Fig. 3 we also learn how a second event influences a surface already affected by a preceding one: σ^0 shows the characteristic pattern of decrease and increase, but σ^0 is not increased beyond the typical values of –8 to –11 dB. Towards the end of April, when the melting season starts, σ^0 shows strong and irregular variations.

In summary, this analysis has shown that in the test regions, events of sudden and large σ^0 increase are linked to a strong decrease of the emissivities. These variations occur after surface melt in conjunction with precipitation followed by surface refreezing. Similar studies in other regions of the Arctic as well as in the Antarctic have shown similar changes in σ^0 and in the brightness temperatures (Voss 2002).

Snow metamorphosis

We now address the reason for the observed changes in the dielectric properties of the surface. Since the discussed events are caused by atmospheric effects, it is likely that the uppermost surface layer, i.e. the snow cover, plays a crucial role. The snow depth on Arctic sea ice typically ranges from about 5 to 40 cm (Ledley 1991). Three phases of snow metamorphosis caused by an event can be identified: initial state, melting phase and refreezing.

In the first phase, the snow layer is dry and has low density with small absorption and scattering (Ulaby et al. 1986). It is nearly transparent at the wavelength used here (2.2 cm). Both active and passive microwave mainly stems from the underlying sea ice surface.

When surface melt occurs because of warm

air advection, the liquid water in the snow will aggregate the small crystals to coarsely grained clusters (Massom et al. 2001). This process can be amplified by rain. The liquid water increases the dielectric losses, increases the emissivity and reduces the penetration depth to about one wavelength. Volume scattering becomes negligible, and both emissivity brightness temperature increase (Smith 1998). During an event of few days, the temperature in the deeper snow layers remains below freezing. It can be speculated that, similar to the observations of Haas (2001) in Antarctica, percolating melt and rain water refreezes and forms a rough icy layer in the snow or at the snow–ice interface. The sea ice underneath is not or only slightly affected.

The third phase starts when temperatures decreases below freezing again so that liquid water creating larger grains and voids in the snow layer (Massom et al. 2001). The penetration depth increases again because liquid water is no longer present. The larger grains increase volume scattering resulting in lower emissivity and brightness temperatures.

Results

Geographical distribution of events

The spatial distribution of the events detected is shown in Fig. 1. Medium and dark grey both represent regions of FY. Dark grey indicates areas where at least one event is detected from October to May during the two winter periods under consideration.

Within the seasonal sea ice zone, where FY grows, events occurred in the following regions: the southern and mid-Hudson Bay; the coast of Labrador in the Labrador Sea; Denmark Strait; the Kara Sea, especially between Novaya Zemlya and the Siberian coast and in several bays of the Laptev Sea; in the Sea of Okhotsk along the Russian coast, the Sakalin island and in most parts of the Bering Sea. It is not surprising that events occur in these marginal seas since this is where cyclones advect warm air and rain.

Large-scale estimation of event area

To estimate the error induced by the described meteorological influences on the FY classification, the area of spurious MY detected by the NTA during winter has been estimated when no new MY is formed. To this end we exclude all regions where MY (1) can have survived the last summer or (2) can be advected by ice drift (both marked in light grey in Fig. 1). For the remaining FY area, the MY output of the NTA increase from 0 to 0.3×10^6 km^2 in the entire Arctic region from October 1999 to May 2000 and from October 2000 to May 2001, respectively, due to falsely detected MY. Note that this MY area correction corresponds to a much larger total area affected because the error in MY concentration during an event is between 10 and 20 %, with initial values up to 40 % (Fig. 2c). The FY area correction accounts for about 13 % of the total area where an event is detected (2.3×10^3 km^2) according to the two criteria that σ^0 (1) increases by more than 3 dB within 4 days and (2) reaches values of –11 dB or higher.

The total ice-covered area of the whole Arctic Ocean reaches about 12×10^6 km^2 in mid-winter. The MY area estimated by the NTA is approximately 2.5×10^6 km^2, most of it being the real MY of the central Arctic. But as shown here about 12 % of the total Arctic MY calculated with the NTA is an artefact and should be replaced by FY.

Assuming a static mask for the MY area is conservative because areas containing mixtures of FY and MY are also excluded from the correction scheme. Therefore, future applications, e.g. aiming at improved time series of MY concentrations and extent, should include a more sophisticated, dynamic discrimination between FY and MY. This will lead to even larger corrections. The correction of the passive microwave data for the period when K_u-band scatterometer data are available appears straightforward, and the correction of the complete 20-year data set of passive microwave imagery, which would have to be based on the data themselves, especially the GR (Fig. 2), could be optimized with data of the overlap period of both sensors.

Conclusions

As sea ice ages, its microwave radiative and backscatter properties are modified. In particular, multi-year sea ice (MY) has a lower emissivity than first-year sea ice (FY) because desalination reduces dielectric loss. The lowering of emissivity depends on the frequency and is exploited by the

NTA to discriminate FY from MY. Furthermore, MY backscatter (>–11 dB) is larger than that of FY (<–11 dB) because of both increased surface roughness at microwave wavelength scale and increased volume scattering due to air pockets. In this study, using routine meteorological information, it is shown how and why melt–refreezing events, enhanced by rain, alter the normal microwave signature of sea ice. The NTA will underestimate the amount of FY and overestimate the amount of MY while the total sea ice concentration remains unchanged. An alternative possibility of a rapid backscatter increase of FY not discussed in this study is ice compression with an associated increase in roughness and ridging. The addition of backscatter data allows correcting for this effect and the NTA can be corrected accordingly. As an example, such a simultaneous use of SSM/I and QSCAT data has been performed in the Arctic seasonal sea ice zone, where most of these events were detected during two consecutive winter periods. The correction amounts to up to 12 % of the area.

Acknowledgements.—SSM/I data were provided by the National Snow and Ice Data Center, University of Colorado, Boulder and the SeaWinds/QSCAT maps by IFREMER/CERSAT, Brest. The weather data were provided by WetterOnline GmbH, Bonn. The first author acknowledges a grant from EUMETSAT for supporting his stay at Institut Français de Recherche pour l'Exploitation de la Mer, Brest.

References

Bingham, A. W. & Drinkwater, M. 2000: Recent changes in the microwave scattering properties of the Antarctic ice sheet. *IEEE Trans. Geosci. Rem. Sens. 38*, 1810–1820.

Cavalieri, D., Crawford, J., Drinkwater, M., Eppler, D., Farmer, L. Jentz, R. & Wackerman, C. 1991: Aircraft active and passive microwave validation of sea ice concentration from the Defense Meteorological Satellite Program Special Sensor Microwave Imager. *J. Geophys. Res. 96(C12)*, 21 989–22 008.

Ezraty, R. 1999: Arctic sea ice microwave signatures. A Lagrangian approach during the NSCAT mission. In: *IGARSS '99 Hamburg Germany: IEEE 1999 International Geoscience and Remote Sensing Symposium, 28 June–2 July 1999—Congress Centrum Hamburg; remote sensing of the system Earth—a challenge for the 21st century; proceedings*. Pp. 1585–1587.

Ezraty, R. & Cavanié, A. 1999: Intercomparison of backscatter maps over Arctic sea ice from NSCAT and ERS scatterometer, *J. Geophys. Res. 104(C5)*, 11471–11483.

Ezraty, R. & Piollé, J. F. 2001: *SeaWinds on QuickSCAT polar sea ice grids—user manual. Convection Report 5, V1.1, August 2001*. Brest: Institut Français de Recherche pour l'Exploitation de la Mer. Available on the internet at www.ifremer.fr/cersat/activite/ceo/imsi/f4i_html/e_ intro.htm.

Gloersen, P., Campbell, W., Cavalieri, D., Comiso, J., Parkinson, C. & Zwally, H. J. 1992: Arctic and Antarctic sea ice, 1978–1987: satellite passive-microwave observations and analysis. Washington, D.C.: National Aeronautics and Space Administration.

Gohin, F. & Cavanié, A. 1994: A first try at identification of sea ice using the three beam scatterometer of ERS-1. *Int. J. Remote Sens. 15*, 1221–1228.

Haas, C. 2001: The seasonal cycle of ERS scatterometer signatures over perennial Antarctic sea ice in summer. *Ann. Glaciol. 33*, 69–73.

Hollinger, J. P., Peirce, J. L. & Poe, G. A. 1990: SSM/I instrument evaluation. *IEEE Trans. Geosci. Remote Sens. 5*, 781–790.

Johannessen, O., Shalina, E. V. & Miles, M. W. 1999: Satellite evidence for an Arctic sea ice cover in transformation. *Science 286*, 1937–1939.

Kwok, R., Comiso, J. C. & Cunningham, G. F. 1996: Seasonal characteristics of the perennial sea ice cover of the Beaufort Sea. *J. Geophys. Res. 101(C12)*, 28 417–28 439.

Kwok, R., Cunningham, G. F. & Yueh, S. 1999: Area balance of the Arctic Ocean perennial ice zone: October 1996 to April 1997. *J. Geophys. Res. 104(C11)*, 25 747–25 759.

Ledley, T. S. 1991: Snow on sea ice: competing effects in shaping climate. *J. Geophys. Res. 96(D6)*, 17 195–17 208.

Liu, G. & Curry, J. 2003: Observation and interpretation of microwave cloud signatures over the Arctic Ocean in winter. *J. Appl. Meteorol. 42*, 51–64.

Martin, T. & Augstein, E. 2000: Large-scale drift of Arctic sea ice retrieved from passive microwave satellite data. *J. Geophys. Res. 105(C4)*, 8775–8788.

Massom, R., Eicken, H., Haas, C., Jeffries, M. O., Drinkwater, M., Sturm, M., Worby, A., Wu, X., Lythe, V., Ushio, S., Morris, K., Reid, P., Warren, S. & Allison, I. 2001: Snow on Antarctic sea ice. *Rev. Geophys. 39*, 413–445.

Parkinson, C. L., Cavalieri, D. J., Gloersen, P., Zwally, H. J. & Comiso, J. C. 1999: Spatial distribution of trends and seasonality in the hemispheric sea ice covers: 1978–1996. *J. Geophys. Res. 104(C9)*, 20 827–20 835.

Serreze, M., Walsh, J., Chapin, F., Osterkamp, T., Dyurgerov, M., Romanovsky, V., Oechel, W., Morrison, J., Zhang, T. & Barry, R. G. 2000: Observational evidence of recent changes on the northern high-latitude environment. *Clim. Change 46*, 159–207.

Smith, D. M. 1998: Observation of perennial Arctic sea ice melt and freeze-up using passive microwave data. *J. Geophys. Res. 103(C12)*, 27 753–27 769.

Ulaby, F. T., Moore, R. & Fung, A. K. 1986: *Microwave remote sensing, active and passive. Vol. III.* Norwood, MA: Artech House.

WetterOnline GmbH 2001: On the internet at www.wetteronline.de, 15 December 2001.

Voss, S. 2002: *Synergetische charakterisierung von meereis mit SSM/I- und Scatterometerdaten. (Synergetic characterization of sea ice with SSM/I- and scatterometer data.)* PhD thesis, Institute of Environmental Physics, University of Bremen.